1   # Adsorption capacity of the corrosion products of

2   # nanoscale zerovalent iron towards emerging contaminants

3

4   Junmin Deng[1,2], Sungjun Bae[2], Sunho Yoon[2], Mathieu Pasturel[3], Rémi Marsac[4],

5   Khalil Hanna[1,5*]

6

7   *[1] Univ. Rennes, Ecole Nationale Supérieure de Chimie de Rennes, CNRS, ISCR-UMR*

8   *6226, F-35000, Rennes, France*

9   *[2] Department of Civil and Environmental Engineering, Konkuk University, 120*

10   *Neungdong-ro, Gwangjin-gu, Seoul 05029, Republic of Korea*

11   *[3] Univ. Rennes, CNRS, ISCR – UMR 6226, F-35000, Rennes, France*

12   *[4] Univ. Rennes, CNRS, Géosciences Rennes – UMR 6118, F-35000 Rennes, France*

13   *[5]Institut Universitaire de France (IUF), MESRI, 1 rue Descartes, 75231 Paris, France*

14   *Corresponding author: khalil.hanna@ensc-rennes.fr

15

16

17

18

19

20

21 **Abstract**

22   Despite the extensive use of nanoscale zerovalent iron (NZVI) in water and soil

23 remediation, no data exist on the reactivity of secondary iron minerals formed upon the

24 NZVI corrosion. Herein, we investigated the oxidation kinetics of NZVI by monitoring

25 the variations of pH, oxidation−reduction potential (ORP) and dissolved Fe(II)

26 concentration, and then examined the reactivity of resulting oxidized particles for the

27 adsorption of an emerging contaminant (nalidixic acid (NA)). NA adsorption was found

28 greatest onto oxidized particles and negligible on the fresh NZVI. Interestingly, the

29 formed secondary mineral phases exhibited an unusual pH adsorption-curve with an

30 unexpected great adsorption at alkaline pH values. X-ray photoelectron spectroscopy

31 and high resolution-transmission electron microscopy revealed a gradual increase in

32 Fe(II) content at the surface of magnetite phase over the reaction time. Additional

33 experiments and surface complexation modeling showed that the enhanced adsorption

34 of NA onto the secondary magnetite is due to the formation of surface bound Fe(II).

35 Fe(II) release into solution because, for instance, of the presence of organic buffer

36 molecules, decreased surface Fe(II) and then NA adsorption at alkaline pH values. This

37 work sheds light on an overseen aspect of the reactivity of secondary iron minerals

38 resulting from NZVI passivation, which can bind co-exiting emerging contaminants

39 and then affect their fate in the environment.

1. Introduction

41   Because nanoscale zerovalent iron (NZVI) is an environmentally-safe material and

42 exhibits great particle reactivity, it has been widely used in treatment processes of

43 various organic and inorganic contaminants [1-3]. As a result, NZVI has become one of

44 the most extensively studied nanomaterials in wastewater treatment and remediation of

45 soil and groundwater.[4-7]

46   For the remediation action, the NZVI slurry is directly introduced into soil and

47 groundwater systems, and NZVI particles migrate from the injection points to affected

48 zones.[8] During this journey, NZVI could encounter many electron acceptors resulting

49 in partial or complete oxidation of NZVI particles (also called surface passivation).

50 These electron acceptors may include oxygen as in oxic environments, nitrate, etc. and

51 targeted compounds, *i.e.* contaminants.[9-12] This oxidation can lead to either formation

52 of Fe^{II}-bearing phases on the NZVI surface or complete oxidation to ferric

53 (oxyhydr)oxides, depending upon various factors including type and concentration of

54 co-existing species, reaction time and oxic/anoxic environments. For instance,

55 lepidocrocite, magnetite and maghemite appeared to be the main secondary iron

56 minerals formed upon the oxic corrosion of NZVI.[13]

57   Although the ability of NZVI to reductively transform a wide variety of compounds

58 has been extensively investigated, little is known about the fate of injected NZVI

59 particles in natural systems. In addition, NZVI passivation byproducts have been

3

60   identified under oxic and anoxic conditions,[14] but no data exist on the reactivity of these

61   byproducts in nature. Indeed, the passivation byproducts (i.e., secondary Fe minerals)

62   would continue to migrate in environmental settings and potentially meet other types

63   of contaminants. They could bind co-existing contaminants and then influence their

64   aqueous or colloidal transport in soil and groundwater. Comprehensive examination of

65   the reactivity of these "abandoned" particles and their mobility in natural settings is

66   essential for ecological risk assessments.

67   Here, we examined the interactions between NZVI (fresh or passivated) and

68   nalidixic acid (NA), a quinolone antibiotic widely used in human and veterinary

69   medicine. NA was selected as a target emerging contaminant because it has been

70   frequently detected in the environment (at concentration levels ranging from $ng \cdot L^{-1}$ to

71    $\mu g \cdot L^{-1}$).[15,16] To control the NZVI oxidation in aqueous suspension, hydrogen peroxide

72   (H_2O_2) was used under anoxic conditions (N_2 glove box). pH and oxidation−reduction

73   potential (ORP) values and dissolved Fe(II) concentration were measured throughout

74   the reaction, and transformation of NZVI particles were monitored by X-ray diffraction,

75   X-ray photoelectron spectroscopy and high resolution-transmission electron

76   microscopy (HR-TEM) equipped with the selected area electron diffraction (SAED).

77   Adsorption tests were performed after total depletion of H_2O_2 in order to prevent any

78   contribution from Fenton-like oxidation (mass balance was also checked) in NA

79   removal. NA adsorption onto the resulting oxidized NZVI particles was evaluated as a

80   function of pH and NA concentration. A surface complexation model was used to

4

81 account for the impact of Fe(II) content on the NA adsorption into secondary Fe

82 minerals.

2. Materials and methods

2.1. Chemicals and materials

85 Nalidixic acid (NA, $\geq$99.0%), sodium borohydride (NaBH$_4$, $\geq$99.0%), ferric

86 chloride hexahydrate (FeCl$_3 \cdot$6H$_2$O, $\geq$99.0%), hydrogen peroxide solution (H$_2$O$_2$, 30%),

87 ferrous chloride tetrahydrate (FeCl$_2 \cdot$4H$_2$O, $\geq$99.0%), 1,10-phenanthroline ($\geq$99.0%),

88 acetic acid ($\geq$99.5%), hydrochloric acid (HCl, 37%), sodium hydroxide (NaOH,

89 $\geq$99.0%), glycerol ($\geq$99.5%), tetracycline hydrochloride (TET, $\geq$99.0%), 4-

90 morpholineethanesulfonic acid (MES, $\geq$99.5%), 4-(2-hydroxyethyl)piperazine-1-

91 ethanesulfonic acid (HEPES, $\geq$99.5%), tris(hydroxymethyl)aminomethane (TRIZMA

92 base, $\geq$99.9%) and Tris(hydroxymethyl)aminomethane hydrochloride (TRIZMA HCl,

93 $\geq$99.5%) were all purchased from Sigma-Aldrich, France. Leonardite Humic Acid

94 standard (LHA) was purchased from the International Humic Substances Society

95 (IHSS). Maghemite (γ-Fe$_2$O$_3$) was purchased from Alfa Aesar, with a high purity

96 (>99.0%). Magnetite (Fe$_3$O$_4$), hematite (α-Fe$_2$O$_3$) and lepidocrocite (γ-FeOOH) were

97 synthesized as previously reported.[17] Acetonitrile (99.99%, Sigma) and acetic acid

98 (99.7%, ACROS) were used for mobile phase of high-performance liquid

99 chromatography (HPLC). NA stock solution (5 mM) and ferrous chloride stock solution

100 (100 mM) were prepared with 0.1 M NaOH and 0.1M HCl, respectively. Glassware

5

101   was soaked in a 5% (v/v) HCl container for at least 48 h and rinsed before use. Unless

102   specifically stated, all solutions were prepared with deoxgenated deionized water

103   (DDIW, 18.2 MΩ·cm) prepared by purging with nitrogen (N_2, 99.99%) for 4 hours and

104   stored in anaerobic chamber (JACOMEX).

105

106   **2.2. Synthesis and characterization of NZVI**

107   NZVI was synthesized following our previous work.[18] Briefly, 500 mL of sodium

108   borohydride solution (0.9 M) was added dropwise into the 500 mL of ferric chloride

109   hexahydrate solution (0.11 M) a fixed rate of 1 mL/min in anaerobic chamber. After

110   finishing the synthesis, the precipitates in the suspension were separated by magnet,

111   then washed 3 times with DDIW. The obtained NZVI was dried and stored inside the

112   anaerobic chamber.

113   The oxidized particles were then analyzed by X-ray diffraction (XRD, D8,

114   BRUKER). The oxidized NZVI suspensions were washed with DDIW for three times,

115   and dried in a vacuum freeze drier (-52℃, 24 h). Then, the dried samples were

116   transferred to sample holders and treated with 1:1 (v:v) glycerol solution to avoid the

117   surface oxidation during the analysis of XRD.[19] X-ray photoelectron spectroscopy

118   (XPS, Sigma Probe system, Thermo) analysis was performed for four different samples

119   (i.e., pristine NZVI, NZVI after reaction with H_2O_2 (3, 15, and 18 h). We used the power

120   source (Al Kα X-ray, 1486.7 eV) of 75 W and the C 1s peak at 285 eV as a reference

121   for correction of surface charging effects. The morphological characterization of

122 different oxidized NZVIs were investigated by high resolution-transmission electron

123 microscopy (HR-TEM, JEM-2100, JEOL) equipped with the selected area electron

124 diffraction (SAED). The specific surface area of oxidized NZVIs was analyzed by

125 multi-point N_2 adsorption isotherm (Micromeritics, USA). The average particle size

126 and zeta potential of the oxidized NZVI particles were measured by Zetasizer MAS

127 (Matec Applied Sciences).

128

129 **2.3. Analytical methods**

130　　Batch experiments were conducted in 500 mL flasks in anaerobic chamber to avoid

131 the effect of dissolved oxygen during the reaction. 0.1 g NZVI was transferred to the

132 flask containing 500 mL DDIW with stirring at 600 rpm to prepare an initial NZVI

133 dosage of 200 mg/L. A portable pH-ORP meter (HANNA, HI991003) was used to

134 monitor the variations in pH and ORP during the oxidation and adsorption processes.

135 After a steady state was reached for both pH and ORP, exact amounts (0.25, 0.5, 1, 2.5

136 or 5 mL) of H_2O_2 stock solution (1 M) were introduced into the suspensions to prepare

137 different oxidized NZVIs by different H_2O_2 concentration at 0.5, 1, 2, 5 or 10 mM,

138 respectively. After reaching the equilibrium of pH and ORP again, 1 mL of NA stock

139 solution (5 mM) was transferred into the suspension to initiate the adsorption of NA (10

140 μM) by the oxidized NZVI. At the sampling times, 1 mL samples were taken from the

141 suspension and filtered through a 0.2 μm filter (Whatman) for analysis of high-

142   performance liquid chromatography (HPLC). After finishing 2-h adsorption, desorption

143   tests were carried out at pH 12 to check the mass balance of NA (Table S1).

144   Aqueous concentration of NA was determined using HPLC (Waters 600 Controller)

145   equipped with a photodiode array detector operating at 258 nm (Waters 996) and a

146   reversed-phase C18 column (250 mm $\times$ 4.6 mm i.d., 5 μm). The mobile phase was a

147   mixture of acetonitrile/water (60/40 v/v) containing 0.1% formic acid. The flow rate of

148   the mobile phase was set at 1 mL/min in isocratic mode.[20] The dissolved Fe(II)

149   concentration was measured by a 1,10-phenanthroline method at a wavelength of 510

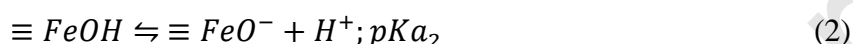150   nm using an UV–vis spectrophotometer (U-3310, HITACHI).

151   The same procedure was used to investigate the oxidation of NZVI in buffered

152   systems. A constant Good's buffer (MES, HEPES and TRIZMA) concentration of 10

153   mM was used to maintain the pH at 5.6, 7.0 and 9.0, respectively[21-22]. These buffers

154   were introduced into the reactor together with NZVI (200 mg/L).

155   All experiments were performed in triplicates, and the data reported here were the

156   average of three replicated experiments and error bars represent the relative standard

157   deviation.

158

159   **2.4. Surface Complexation Modeling**

160   The NA removal in the NZVI suspension at different pH values were described

161   using surface complexation modeling. The geochemical speciation code PHREEQC

162   and the "minteq" database were used.[23] The pK$_a$ of NA is 6.19 and the logarithm of the

8

163   formation constant of NA−Fe$^+$(aq) is 3.99.[24] The surface complexation models for

164   magnetite are used, as previously reported, [25] and the protonation of Fe surface sites is

165   formulated following a 2-pK$_a$ approach (Eqs. (1) and (2)).

166

167               $\equiv FeOH_2^+ \leftrightharpoons \; \equiv FeOH + H^+; pKa_1$ (1)

168               $\equiv FeOH \leftrightharpoons \; \equiv FeO^- + H^+; pKa_2$ (2)

169
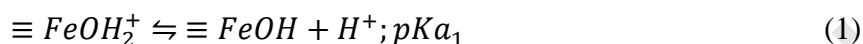
170   Charge-potential relationship was described according to the constant capacitance

171   model (CCM), and the modeling parameters are presented in the supporting information

172   (Table S2). Though the CCM is not available in PHREEQC (version 2), we have

173   adapted parameters of the three plane model (TPM) implemented in PHREEQC in

174   order to use the CCM, as previously reported.[26]

175

176   3.   **Results and discussion**

177   **3.1. NZVI oxidation in aqueous solution and NA removal**

178   Variations in pH, ORP and dissolved Fe(II) concentration were monitored during

179   i) the addition of NZVI in reactor, ii) the oxidation of NZVI by H$_2$O$_2$, and iii) the

180   removal of NA by the resulting secondary particles (Figure 1). When NZVI was added

181   in water (i.e., the first 2-h period), we observed an obvious increase in pH (from 6.9 to

182   8.9) and a decrease in ORP (from 81 to -748 mV), which can be attributed to generation

9

183   of OH⁻, Fe^{2+}, and H_2 during the anaerobic corrosion of NZVI (Eq.(3)).[27]

184

185
$$Fe^0 + 2H_2O \rightarrow Fe^{2+} + 2OH^- + H_2 \qquad (3)$$

186
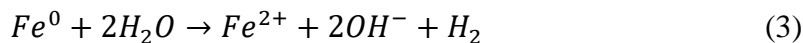
187   After adding H_2O_2 into the NZVI suspension, the ORP value increased rapidly up

188   to 241 mV due to the standard potential of H_2O_2/ H_2O (1.37 V)[28], while pH dropped to

189   7.8 which is ascribed to the oxidation and hydrolysis of released iron ions. In addition,

190   the release of H^+ from H_2O_2 dissociation (pK_a of 11.6) presumably results in pH

191   decrease.[29]

192
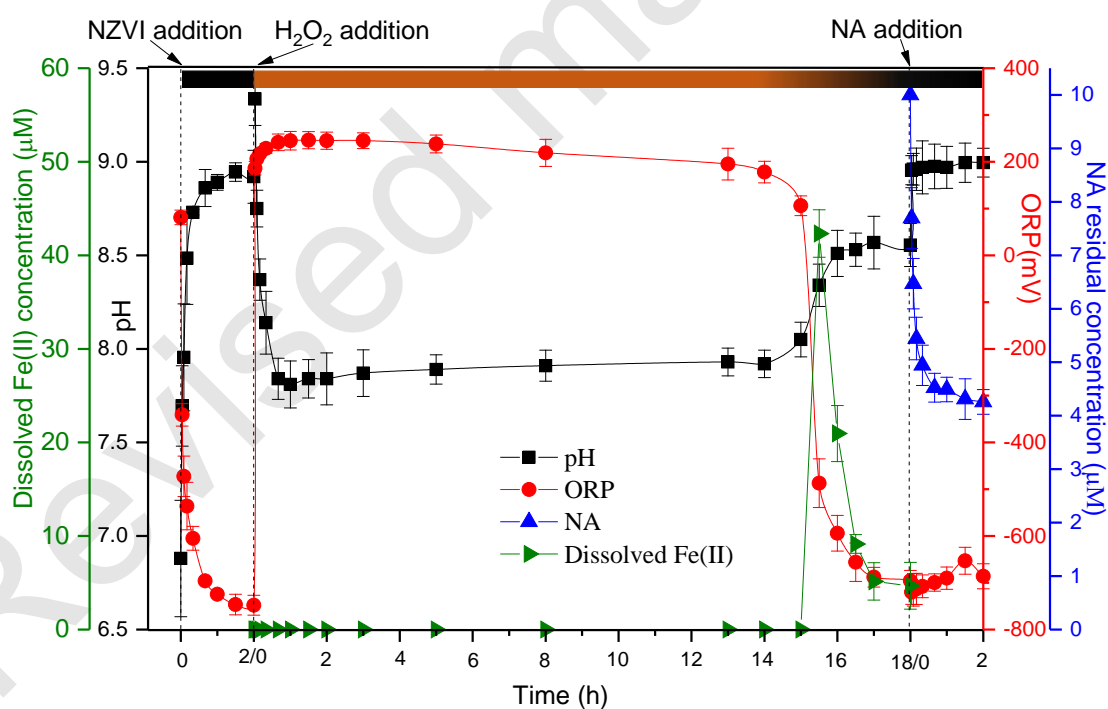
193   **Figure 1**. Variations in pH, ORP, color of suspension, dissolved Fe(II) concentration
194   and NA concentration during the NZVI oxidation and NA adsorption. Experimental
195   conditions: [NZVI] = 0.2 g·L⁻¹, [H₂O₂] initial = 5 mM, [NA]initial = 10 μM, 20 ±1 °C.

196   After a long steady-state period for both ORP and pH values (around 15 h), ORP

197   decreased sharply until -696 mV and the pH increased to 8.6, which can be attributed

198   to the complete consumption of H_2O_2 (as it is also verified by   the molybdate-catalyzed

199   iodometric titration method[30]). During the reaction between H_2O_2 and NZVI, protons

200   are consumed (Eq. (4)),[31,32] which can balance the protons generated as a result of

201   hydrolysis of Fe(III). The latter is generated from the rapid oxidation of ferrous species

202   in the presence of H_2O_2, which has been experimentally checked by the no detection of

203   dissolved Fe(II) during that period.

204

205    $$Fe^0 + H_2O_2 + 2H^+ \leftrightharpoons Fe^{2+} + 2H_2O \qquad (4)$$

206
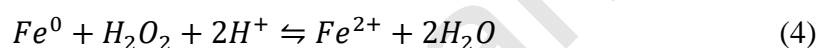
207   Once H_2O_2 was totally consumed and ORP reached again negative values, release of

208   dissolved Fe(II) into solution was observed. Then, the dissolved Fe(II) concentration

209   decreased over reaction time, likely due to adsorption to oxide particles, particularly at

210   high pH value (~8). It is worth noting that the color of suspension changed from black

211   to yellow after the addition of H_2O_2, and gradually turned to black after the 15-h

212   reaction.

213   Once the ORP and pH values reached steady-state values, a desired concentration

214   of NA was introduced into the reaction system, and residual NA concentration was

215   monitored over time (Figure 1). A slight increase in pH can be mainly attributed to the

216   alkalinity of the NA mother solution, but also to NA binding to oxide surfaces. Indeed,

11

217   almost 60% of NA removal was observed after 2 h of reaction time at the working pH

218   (~9). NA removal by, for instance, Fenton-like oxidation is excluded under our

219   experimental conditions, since full mass balance was achieved at the end of reaction,

220   *i.e.* desorbed amounts equivalent to adsorbed ones (Table S1). This great adsorption

221   (~29 µmol per g of initial NZVI added) at an alkaline pH is quite unusual, and thus not

222   comparable with the typical pH-dependence behavior of adsorption of

223   monocarboxylates or polyfunctional compounds, as for example quinolones.[20] Indeed,

224   the sorption behavior of such compounds to metal oxides is generally attributed to a

225   combination of pH-dependent speciation of compound (*e.g.* pK_a of NA = 6.19) and

226   surface charge characteristics of the mineral oxide (PZC of Fe-oxyhyrdoxides is

227   generally between 8 and 9.5).[20] As a result, adsorption is generally high at low pH value

228   and then decreases when pH increases, and becomes negligible at pH higher than 10.[33]

229   Here, the NA adsorption is unusually high at pH around 9, and even increased from 29

230   to 40 µmol/g when the initial NA concentration increased from 10 to 20 µM, further

231   confirming the high affinity of the NZVI oxidation products toward NA.

232

233   **3.2. Secondary minerals formation and impacts on NA removal**

234   NZVI can be oxidized and/or transformed into different iron oxides depending on

235   the oxidant dose, which may exhibit contrasting affinities towards NA. For this reason,

236   additional experiments of NZVI oxidation were performed with different H_2O_2

237   concentrations (Figure S1). Generally, higher H_2O_2 concentration led to a rapid increase

238   in ORP value in NZVI suspension, and then decrease to reach the initial value, except

239   for the highest H_2O_2 dose. For the sake of clarity, only the last stage, *i.e.* NA adsorption,

240   was shown and the adsorbed amount of NA was plotted versus time for different H_2O_2

241   concentrations (0 - 10 mM) (Figure 2a). Interestingly, a negligible removal of NA was

242   observed on the fresh NZVI, while the NA removal amount onto the resulting secondary

243   minerals increased with increasing in H_2O_2 dose, yet no significant difference was

244   observed for the two highest doses (5 and 10 mM). It is interesting to note that the NA

245   removal amount by the corrosion particles of NZVI can be enhanced in the presence of

246   humic acid (LHA was used here as model of natural organic matter) (see Figure S3).

247   Indeed, the presence of 5 mg/L of LHA increased the NA adsorbed amount from 22 to

248   30 µmol/g. This enhanced adsorption in the presence of humic acids can be ascribed to

249   better dispersion of secondary mineral particles, thus increasing available surface area

250   as previously reported.[34]

251
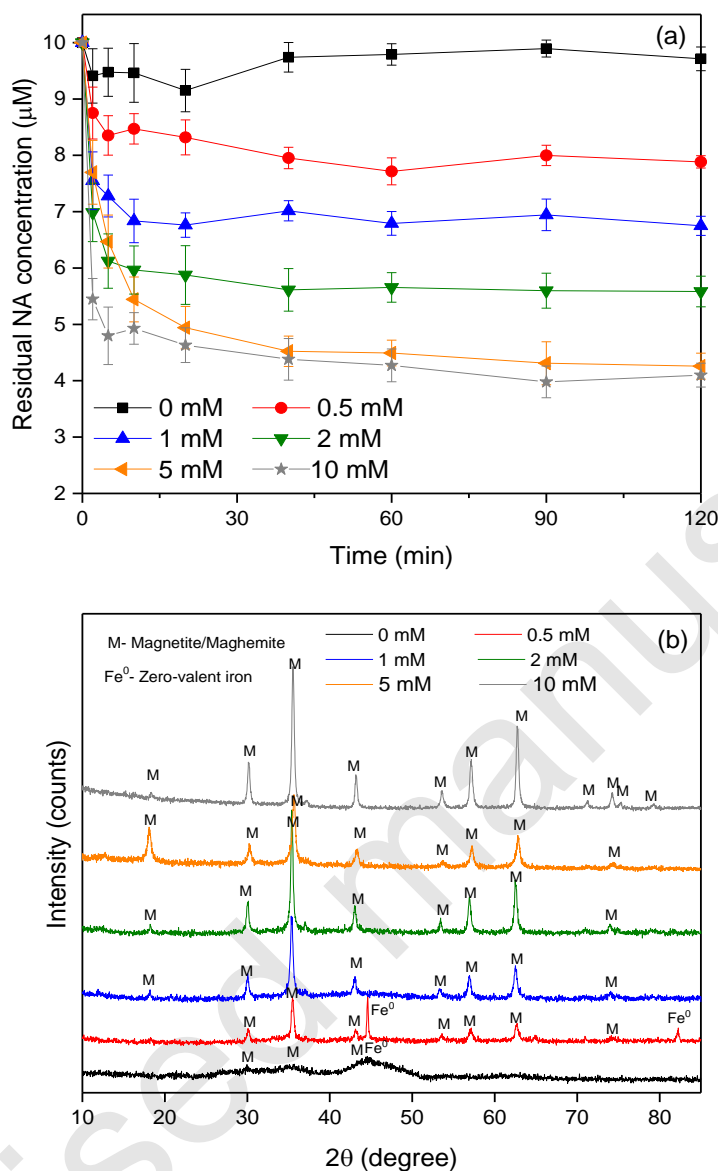
Figure 2. (a) NA removal by the oxidation NZVI samples (b) XRD patterns of secondary minerals at different H_2O_2 concentrations (0 - 10mM); unbuffered systems (pH= 9 ±0.2 for the adsorption stage); [NZVI]=0.2 g·L^{-1}, [NA]$_{initial}$=10 µM, 20 ±1 °C.

255

As the adsorption capacity is closely related to the properties of iron oxides and hydroxides, the resulting secondary minerals were firstly characterized by XRD (Figure 2b). The XRD pattern of fresh NZVI revealed the presence of a broad peak of α-Fe

14

259   (44.5° 2θ) with weak peaks of magnetite and/or maghemite (marked as M) due probably

260   to outer iron oxide shell of NZVI particles.[18] At low H_2O_2 concentration (0.5 mM),

261   peaks of α-Fe were still observed while new peaks corresponding to magnetite and/or

262   maghemite appeared. At H_2O_2 concentration over 1 mM, magnetite/maghemite was

263   detected as the major secondary iron minerals (Figure 2b).

264   To gain more insight about potential changes in surface properties upon NZVI

265   oxidation, zeta potential and average particle size of the secondary mineral particles

266   were measured. These results showed that H_2O_2 induced oxidation may influence the

267   aggregation behavior in NZVI suspension (Figure S2). While Zeta potential negative

268   value is within the reported values for bare NZVI at alkaline pH (9),[35] H_2O_2 induced

269   oxidation resulted in a significant reduction of the mean size of agglomerates from

270   around 4000 nm to around 800 nm when the H_2O_2 concentration exceeded 2 mM.

271   However, the zeta potential of NZVI suspension did not change significantly over the

272   entire H_2O_2 concentration range. Generally, increasing in negative surface charge of

273   particles may indicate dispersion or lower aggregation.[36] Here, enhancement in the

274   electrostatic repulsion effect and thus the dispersion of the particles is only observed at

275   higher H_2O_2 dose, that could be associated with the formation of magnetite/maghemite

276   particles (Fig. 2b). The high agglomeration observed for the fresh NZVI or slightly

277   oxidized NZVI could be possibly due to electrostatic attractions between various kinds

278   of particles: Fe^0, iron oxides coating the Fe^0 core and other secondary minerals.

279   Furthermore, the van der Waals interactions between these particles may take place

280 because of the limited electrostatic repulsion between particles. Accordingly, the BET

281 surface area of the oxidized particles (using 5 mM of H_2O_2) (28.2 ± 1.5 m^2/g) was found

282 almost twice higher than the surface area of the fresh NZVI (14.9 ± 1 m^2/g).

283 Collectively, these results suggest that fresh NZVI (or Fe^0) has negligible affinity

284 for NA adsorption, and the secondary Fe minerals could be responsible of the NA

285 removal in NZVI suspension.

286

287 **3.3. Structural evolution of NZVI over reaction time**

288 As the highest removal rate of NA was observed with a high dose of H_2O_2 (5 or

289 10 mM), we have investigated the morphological changes of oxidized NZVI particles

290 over reaction time when 5 mM of H_2O_2 was used for oxidation. Two key stages of NZVI

291 oxidation kinetics were investigated (as shown in Figure 1) : (i) 3h, after H_2O_2 addition

292 and when ORP and pH values have reached a plateau (oxidizing conditions), and (ii)

293 18h just before NA addition and when ORP and pH values have reached constant values

294 after complete H_2O_2 depletion.

295

16
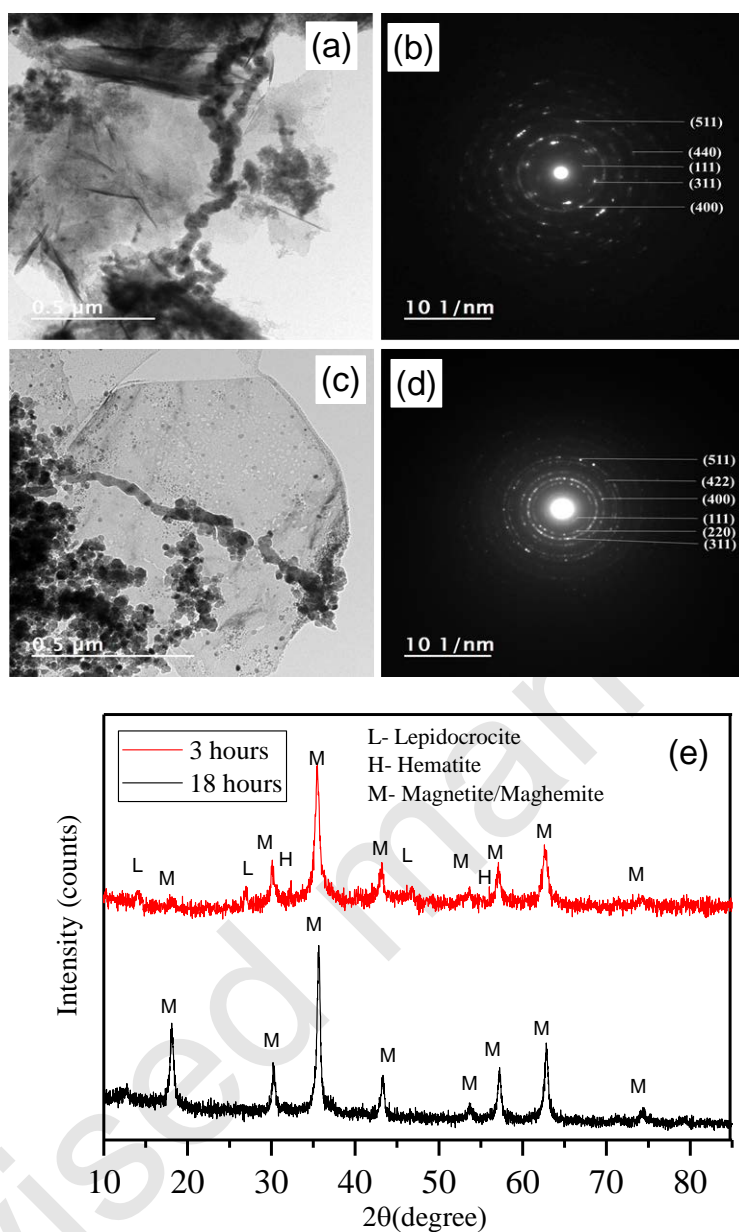
Figure 3. TEM images and SEAD pattern of the oxidized NZVI with 5 mM H_2O_2 at two oxidation times (a and b) 3 hours and (c and d) 18 hours, and (e) corresponding XRD patterns.

In the 3-h sample, we observed the presence of chain-like aggregates of nanoparticles

and needle-like shaped individual nanoparticles (Figure 3). The SAED pattern of chain-

303   like aggregates (Figure 3b) showed the d-spacing of 4.87, 2.53, 2.09, 1.60 and 1.49 Å,

304   which are assigned to the (111), (311), (400), (511), and (440) of magnetite/maghemite

305   phase, respectively.[37] In addition, the XRD of 3-h sample revealed the presence of peaks

306   of magnetite/maghemite, lepidocrocite, and hematite (Figure 3e). This is consistent

307   with previous investigation, which showed that needle-shaped lepidocrocite was

308   formed as a secondary product from NZVI oxidation in oxygenated water.[38] TEM

309   image of 18h oxidized NZVI (Figure 3c) shows the presence of nanoparticles

310   aggregates without other distinct shaped particles. Single nanoparticles (20 nm as an

311   average size) were connected to form chain-like magnetic nanoparticles (see Figure S4).

312   The SAED pattern of these aggregates revealed the reflections of (111, 4.87 Å), (220,

313   2.98 Å), (311, 2.53 Å), (400, 2.08 Å), (422, 1.70 Å), and (511, 1.59 Å), corresponding

314   to magnetite or maghemite.[39] Though these minerals both have indistinguishable

315   diffraction patterns, the chain-like assembly of these nanoparticles may suggest strong

316   ferromagnetic properties of particles at room temperature. Because the weak dipole–

317   dipole interactions between the maghemite particles are usually not sufficient to result

318   in the chain formation, the chain assemblies observed here tend to support the formation

319   of magnetite as the dominant phase.[40,41] This falls in line with previous report,[42] where

320   magnetite has been detected as the major secondary iron mineral under anoxic

321   conditions (*i.e.* equivalent to conditions here within the 15h-18h period of reaction). In

322   addition, the oxidation of NZVI to magnetite (Fe_3O_4) seems to be more

323   thermodynamically favorable at alkaline pH values.[23,43]

324
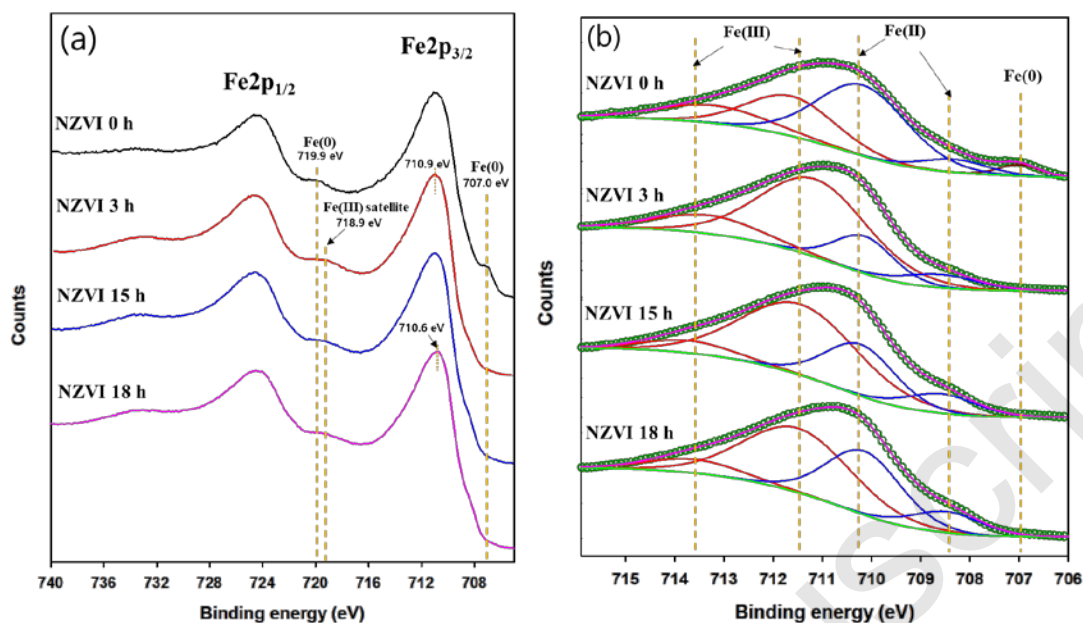
325 **Figure 4.** XPS spectra for (a) Fe2p of NZVI before and after reaction with H_2O_2 and

326 (b) and the deconvolution results of Fe2p$_{3/2}$ (706−716 eV). Conditions: $[H_2O_2]$ = 5 mM,

327 [NZVI]=0.2 g·L^{-1}

328

329   XPS analyses were conducted on NZVI samples oxidized with 5 mM of H_2O_2 at

330 different reaction times (0, 3, 15 and 18h). The XPS spectra for Fe2p$_{3/2}$ (Figure 4(b))

331 were composed of five different peaks at 707.0, 708.3−708.5 eV, 710.1−710.3,

332 711.1−711.6, and 713.2−713.7 eV, which are assigned to the binding energies for Fe(0)

333 (706.5−707.0 eV), Fe(II)-O (708.2−710.9 eV), and Fe(III)-O (711.0–714.0 eV),

334 respectively.[44] In the pristine NZVI, two distinct peaks were observed at 719.9 and 707

335 eV, corresponding to Fe2p$_{1/2}$ and Fe2p$_{3/2}$ of Fe(0), respectively (Figure 4(a)).[45] After 3-

336 h reaction, we observed the disappearance of Fe(0) peaks and the formation of new

337 Fe(III) satellite peak at 718.9 eV, indicating the presence of Fe(III) minerals (*e.g.*

338 maghemite).[46-48] The proportion of Fe(II) (55.4% → 24.2%) on the NZVI surface

339   decreased after 3 h-reaction whereas that of Fe(III) increased from 41.2% to 75.8%

340   (Figure 4(b)), underscoring the surface oxidation of NZVI by H_2O_2. However, the Fe(III)

341   satellite peak gradually decreased over reaction time (3 to 18 h), whereas the peak of

342    $Fe2p_{3/2}$ shifted to lower binding energy (710.9 $\rightarrow$ 710.6 eV) (Figure 4(a)). The

343   disappearance of Fe(III) satellite peak may result from mineral transformation of Fe^{III}-

344   oxides (e.g. maghemite) into magnetite as previously reported.[48] Indeed, the proportion

345   of Fe(II) increased (34.7% at 15 h to 43.3% at 18 h), and Fe(III) decreased (65.3% at

346   15 h to 56.7% at 18 h) with increasing reaction time (Figure 4b).

347   Based on all experimental findings above, an oxidation pathway of NZVI by H_2O_2

348   can be proposed as two successive steps (Figure S5). In the early stage of NZVI

349   oxidation, highly oxidizing condition caused by the addition of a high dose of H_2O_2 can

350   form mixed valence oxides (*i.e.* magnetite), but also Fe^{III}-oxyhydoxides (lepidocrocite,

351   maghemite and hematite), resulting in change of NZVI suspension color from black to

352   yellowish (Figure 1). After the remained H_2O_2 was completely depleted over 15h of

353   reaction time, reducing conditions (ORP value reached the initial value of fresh NZVI

354   suspension) and then release of ferrous ions into solution concurrently take place

355   (Figure 1). Afterwards, the dissolved ferrous ions tend to re-sorb on the surface of

356   Fe(III)-oxyhydroxides at alkaline pH value, leading to their transformation into

357   magnetite as previously reported for lepidocrocite or hematite (Eqs. (5) and (6)).[49,50]

358

359        $2\gamma FeOOH + Fe^{2+} \rightarrow Fe_3O_4 + 2H^+$ (5)

360     $$\alpha Fe_2O_3 + Fe^{2+} + H_2O \rightarrow Fe_3O_4 + 2H^+ \hspace{2cm} (6)$$
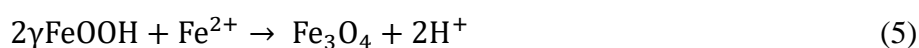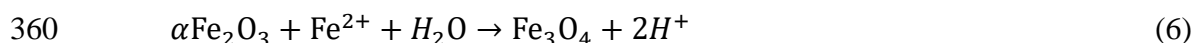
361   Color change from yellowish to black of suspension further suggested such

362   transformation into magnetite phase. Therefore, Fe(II)-release during the oxidation of

363   NZVI suspension and its re-adsorption to secondary minerals may influence the surface

364   reactivity of the resulting products.

365   Additional experiments of NA removal by fresh NZVI or oxidized products (Figure

366   S6) using Good's buffers showed that NA adsorption decreased with pH increasing.

367   However, the NA adsorption at pH 9 was much lower in buffered systems as compared

368   to the un-buffered NZVI suspension (Figure 1). This discrepancy is probably due to the

369   interactions of Good's buffers with the Fe oxide surfaces, which may cause the rapid

370   Fe(0) corrosion and Fe(II) release. [51] It was reported that such Fe(II) release may lead

371   to lepidocrocite formation through Fe(II)-catalyzed transformation of poorly

372   crystallized Fe-oxides (*e.g.* ferrihydrite) and/or oxidation of Fe(II) at acidic-neutral

373   pH.[51] Accordingly, lepidocrocite was identified here as the major phase in buffered

374   NZVI suspension at pH 5.6 and 7 (Figure S7). However, the oxidation products in

375   TRIZMA buffered system (pH 9) were mostly highly amorphous, which makes difficult

376   an accurate identification of secondary iron minerals (Figure S7). It is worth noting that

377   oxidation in TRIZMA buffered system led to dispersion of NZVI particles in suspension

378   and enhancement in zeta potential (Figure S8) compared to that without TRIZMA

379   (Figure S2), thus confirming interactions of TRIZMA molecules with Fe-oxides.

380   Therefore, interactions of organic buffer's molecules with mineral surfaces may affect

21

381   the Fe(II) binding. In the absence of Good's buffers, no elution of Fe(II) is expected

382   and thus the surface bound Fe(II) can be preserved. This is consistent with previous

383   works which showed that organic buffers increased the Fe(II) apparent solubility in

384   goethite and magnetite suspensions even in the alkaline pH range.[21-22] Collectively,

385   these results further suggest that the Fe(II) bound to secondary minerals (i.e. magnetite)

386   could control on the surface reactivity and then the binding capacity toward negatively

387   charged contaminants.

388

389   **3.4. NA adsorption mechanisms on secondary minerals**

390   To check the pH dependence of Fe(II) release and NA sorption onto the NZVI

391   oxidation products, residual concentrations of NA and dissolved Fe(II) in oxidized

392   NZVI suspension were monitored over a wide range of pH (6−11) (Figure 5). NA

393   adsorption was found the greatest between pH 6 and 9, and the lowest between pH 10

394   and 11. This pH adsorption edges differs from the previously reported data of NA

395   adsorption to Fe-oxyhydroxides[20, 26] or the NA adsorption data obtained here with three

396   synthetic Fe-oxyhydroxides (See Figure S9).   Indeed, NA adsorption to non-

397   stoichiometric   magnetite (Fe_3O_4)[26],   goethite $(\alpha\text{-}FeOOH)$[20]   or   other   ferric

398   oxyhydroxides (maghemite, hematite or lepidocrocite) decreased as increasing pH and

399   became negligible for pH higher than 9. Here, the pH-adsorption curve of NA onto

400   NZVI oxidized products shifts to larger pH values, probably because of the presence of

401   dissolved Fe(II). The concentration of dissolved Fe(II) (no dissolved Fe(III) was found)

22

402 decreased as pH increasing. Because of H^+ promoted dissolution of magnetite, Fe(II)

403 dissolution takes place at low pH, which can explain the high amount of dissolved Fe(II)

404 at that pH range.[27] This observation falls in line with a previous investigation on the

405 reactivity assessment of magnetite in presence of variable dissolved Fe(II) amounts [26].

406 Indeed, it was shown that Fe(II) recharge of magnetite enhanced its binding capacity

407 towards organic and inorganic compounds, shifting the maximum sorption to alkaline

408 pH values.[26] Furthermore, Fe(II)-amendment of non-stoichiometric magnetite

409 (Fe(II)/Fe(III) = 0.40) led to similar sorption capacity as compared to the stoichiometric

410 magnetite (i.e. Fe(II)/Fe(III) = 0.50).[26] In the present work, the Fe(II)/Fe(III) ratio of

411 NZVI oxidized products determined by acid digestion was found very high (1.03) and

412 much more than the expected ratio for a magnetite phase, probably because of the

413 presence of residual traces of Fe^0.
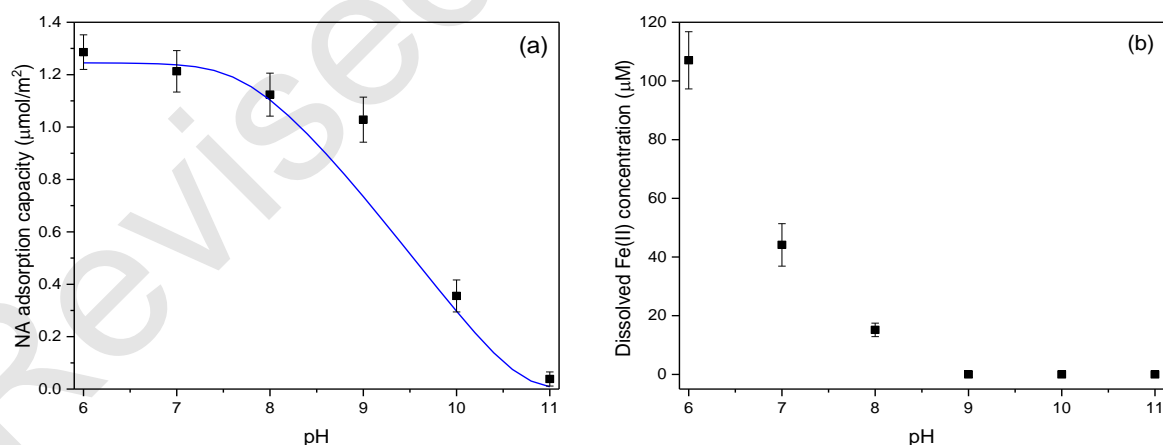
414 **Figure 5.** pH-dependency of (a) NA adsorption and (b) dissolved Fe(II) concentration
415 in NZVI suspension after oxidation (5mM H_2O_2). Lines are modeling results.
416 Experimental conditions: [NZVI]= 0.2 g·L^{-1} ,[NA]= 10 μM, 20 ±1 °C. The BET surface
417 area used here is that measured for the oxidized particles (using 5 mM of H_2O_2) (28.2
418 ± 1.5 m^2/g).

419   In order to confirm the role of surface bound Fe(II) in the enhanced NA binding,

420   we washed the final NZVI products with DDIW for 3 times and then monitored the NA

421   uptake (Figure S10). Sharp decrease of Fe(II)/Fe(III) ratio from 1.03 to 0.61 upon

422   washing of NZVI products indicated strong loss of Fe(II) during the washing process.

423   For NA adsorption at pH 9 (Figure S10), almost 2-fold decrease in adsorbed amount

424   was observed after the washing process, confirming the crucial role of the surface

425   bound Fe(II) in the enhanced NA adsorption.

426   As an attempt to explain the enhanced NA adsorption at high pH with respect to

427   the presence of Fe(II), we used a surface complexation model, previously developed

428   for the stoichiometric magnetite.[26] We assumed that NA binds to two surface hydroxo

429   groups[20, 52] by involving its carboxylate and its keto-group as following:

430

431     $2 \equiv FeOH + 2\,H^+ + NA^- \rightleftharpoons (\equiv Fe)_2NA^+ + 2\,H_2O$ $\quad^SK$ (7)

432

433   As presented in Figure 5, accurate description of experimental results of NA

434   adsorption by the oxidized NZVI particles was obtained at a wide pH range (6−11). We

435   used the measured dissolved Fe(II) concentration at the end of each adsorption

436   experiment as input parameters to account for NA−Fe(II) aqueous complex formation.

437   The good accuracy with the experimental data using the modeling parameters of the

438   stoichiometric magnetite (see Table S2) suggests that magnetite controls NA binding to

439   oxidized NZVI, and further confirms the key role of surface bound Fe(II).

24

440   It is interesting to note that the great binding capacity of the corrosion particles of

441 NZVI at alkaline pH values also concerns other antibiotics of contrasting structure and

442 properties. Indeed, great adsorption of TET (*i.e.* 70% removal of 10μM) onto the

443 oxidized NZVI particles was observed at pH 9.0 ± 0.2 (Figure S11). Taken together,

444 these results highlight the key role of Fe(II) generated along the NZVI oxidation process

445 in promoting greater binding abilities of the secondary minerals.

446

447 **4. Conclusions**

448   NZVI oxidation or passivation in ambient environments can lead to either

449 formation of Fe^{II}-bearing phases on the NZVI surface or complete oxidation to ferric

450 (oxyhydr)oxides. Under the experimental conditions of this study, NZVI oxidation led

451 to formation of Fe^{II}-bearing secondary minerals, with magnetite as the major phase.

452 The latter exhibited higher adsorption ability for organic contaminants, in contrast to

453 the fresh NZVI. In addition, an unexpected great adsorption at alkaline pH values was

454 observed with the formed secondary Fe minerals. This behavior is due to the gradual

455 increase in Fe(II) content at the surface of magnetite phase over the reaction time. A

456 surface complexation model confirmed that NA adsorption onto the secondary

457 magnetite is due to the formation of surface bound Fe(II). If Fe(II) is released into

458 solution, the surface bound Fe(II) decreased together with the NA adsorbed amount at

459 alkaline pH values. As iron (oxyhydr)oxide-coated NZVI particles or Fe(II)-Fe(III)

460 (oxyhydr)oxides may exhibit different adsorption affinities toward negatively charged

461 molecules (e.g. antibiotics) or positively charged compounds, more attention should be

462 paid to the reactivity assessment of passivated NZVI particles or corrosion products.

463 Therefore, the modeling of contaminant fate and transport should consider the impact

464 of these secondary Fe minerals on the mobility of emerging contaminants in soil and

465 groundwater.

466

467 **Conflicts of interest**

468 There are no conflicts to declare.

469

474

475 **Supplementary information**: Additional information regarding oxidation and

476 adsorption kinetics, TEM images and XRD data, additional data on zeta potential and

477 average particle size measurements, and surface complexation model parameters.

References

478 **References**

479 1. S. H. Joo, A. J. Feitz and T. D. Waite, Oxidative Degradation of the Carbothioate
480   Herbicide, Molinate, Using Nanoscale Zero-Valent Iron. *Environ. Sci. Technol.,*
481   2004, *38*, 2242-2247.

482 2. J. Ma, D. He, R. N. Collins, C. He and T. D. Waite, The tortoise versus the hare -
483   Possible advantages of microparticulate zerovalent iron (mZVI) over
484   nanoparticulate zerovalent iron (nZVI) in aerobic degradation of contaminants,
485   *Water Res.*, 2016, **105**, 331-340.

486 3. S. Tsarev, R. N. Collins, E. S. Ilton, A. Fahy and T. D. Waite, The short-term
487   reduction of uranium by nanoscale zero-valent iron (nZVI): role of oxide shell,
488   reduction mechanism and the formation of U(V)-carbonate phases, *Environ. Sci.*
489   *Nano*, 2017, **4**, 1304-1313.

490 4.   D. He, J. Ma, R. N. Collins and T. D. Waite, Effect of Structural Transformation
491   of Nanoparticulate Zero-Valent Iron on Generation of Reactive Oxygen Species,
492   *Environ. Sci. Technol.,* 2016, **50**, 3820-3828.

493 5. T. Liu, X. Li and T. D. Waite, Depassivation of Aged Fe0 by Ferrous Ions:
494   Implications to Contaminant Degradation, *Environ. Sci. Technol.*, 2013, **47**,
495   13712-13720.

496 6. T. Phenrat, T. Thongboot and G. V. Lowry, Electromagnetic Induction of
497   Zerovalent Iron (ZVI) Powder and Nanoscale Zerovalent Iron (NZVI) Particles
498   Enhances Dechlorination of Trichloroethylene in Contaminated Groundwater and
499   Soil: Proof of Concept. *Environ. Sci. Technol.,* 2016, **50**, 872-880.

500 7. Y.-T. Wei, S.-C. Wu, C.-M. Chou, C.-H. Che, S.-M. Tsai and H.-L. Lien,
501   Influence of nanoscale zero-valent iron on geochemical properties of groundwater
502   and vinyl chloride degradation: A field case study, *Water Res.,* 2010, **44**, 131-140.

503 8. C. Su, R.W Pulsa, T. A. Krug, M. T. Watling, S. K. O'Hara, S. K; J. W. Quinnc and
504   N. E. Ruiz, Travel distance and transformation of injected emulsified zerovalent
505   iron nanoparticles in the subsurface during two and half years, *Water Res.*, **47**,
506   4095-4106.

507 9. W. X. Zhang, Nanoscale Iron Particles for Environmental Remediation: An
508   Overview. *J. Nanopart. Res*. 2003, **5**, 323-332.

509 10. B. C. Reinsch, B. Forsberg, R. L. Penn, C. S. Kim and G. V. Lowry, Chemical
510   Transformations during Aging of Zerovalent Iron Nanoparticles in the Presence of
511   Common Groundwater Dissolved Constituents, *Environ. Sci. Technol.*, 2010, 44,
512   3455-3461.

513 11. J.-Y. Ahn, C. Kim, H.-S. Kim, K.-Y. Hwang and I. Hwang, Effects of oxidants on
514   in situ treatment of a DNAPL source by nanoscale zero-valent iron: A field study,
515   *Water Res.*, 2016, **107**, 57-65.

516 12. J. Chen, Z. Xiu, G. V. Lowry and P. J. J. Alvarez, Effect of natural organic matter
517   on toxicity and reactivity of nano-scale zero-valent iron, *Water Res.*, 2011, **45**,

518   1995-2001.

519   13. H. Pullin, R. A. Crane, D. J. Morgan and T. B. Scott, The effect of common
520   groundwater anions on the aqueous corrosion of zero-valent iron nanoparticles and
521   associated removal of aqueous copper and zinc, *J. Environ. Chem. Eng*, 2017, **5**,
522   1166-1173.

523   14. A. Liu, J. Liu, J. Han and W.-x. Zhang, Evolution of nanoscale zero-valent iron
524   (nZVI) in water: Microscopic and spectroscopic evidence on the formation of
525   nano- and micro-structured iron oxides, *J. Hazard. Mater.*, 2017, **322**, 129-135.

526   15. C. Poppe, M. Ayroud, G. Ollis, M. Chirino-Trejo, N. Smart, S. Quessy and P.
527   Michel, Trends in Antimicrobial Resistance of Salmonella Isolated from Animals,
528   Foods of Animal Origin, and the Environment of Animal Production in Canada,
529   1994-1997, *Microb. Drug Resist*, 2001, **7**, 197-212.

530   16. F. Campioni, R. A. Souza, V. V. Martins, E. G. Stehling, A. M. M. Bergamini and
531   J. P. Falcão, Prevalence of gyrA Mutations in Nalidixic Acid-Resistant Strains of
532   Salmonella Enteritidis Isolated from Humans, Food, Chickens, and the Farm
533   Environment in Brazil, *Microb. Drug Resist.*, 2016, **23**, 421-428.

534   17. U. Schwertmann, R. M. Cornell, Iron Oxides in the Laboratory: Preparation and
535   Characterization. Wiley- VCH: New York, 2000.

536   18. S. Bae, S. Gim, H. Kim and K. Hanna, Effect of $NaBH_4$ on properties of nanoscale
537   zero-valent iron and its catalytic activity for reduction of p -nitrophenol, *Appl.*
538   *Catal., B*, 2016, **182**, 541-549

539   19. S. Bae and W. Lee, Influence of Riboflavin on Nanoscale Zero-Valent Iron
540   Reactivity during the Degradation of Carbon Tetrachloride, *Environ. Sci. Technol.*,
541   2014, **48**, 2368-2376.

542   20. J. Xu, R. Marsac, C. Wei, F. Wu, J. F. Boily and K. Hanna, Cobinding of
543   Pharmaceutical Compounds at Mineral Surfaces: Mechanistic Modeling of
544   Binding and Cobinding of Nalidixic Acid and Niflumic Acid at Goethite Surfaces,
545   *Environ. Sci. Technol.*, 2017, **51**, 11617-11624.

546   21. A. Buchholz, C. Laskov and S. B. Haderlein, Effects of Zwitterionic Buffers on
547   Sorption of Ferrous Iron at Goethite and Its Oxidation by CCl_4, *Environ. Sci.*
548   *Technol.*, 2011, **45**, 3355-3360.

549   22. R. Marsac, M. Pasturel and K. Hann, Reduction Kinetics of Nitroaromatic
550   Compounds by Titanium-Substituted Magnetite, *J. Phys. Chem. C,* 2017, **121**,
551   11399-11406.

552   23. D. L. Parkhurst and C. A. J. Appelo, User's guide to PHREEQC (Version 2): A
553   computer program for speciation, batch-reaction, one-dimensional transport, and
554   inverse geochemical calculations, *Water Resources Investigations Report*, 1999,
555   99-4259,

556   24. W. R. Vincent, S. G. Schulman, J. M. Midgley, W. J. van Oort and R. H. A. Sorel,
557   Prototropic and metal complexation equilibria of nalidixic acid in the
558   physiological pH region, Int. J. Pharm., 1981, **9**, 191-198.

559   25.   R. Jolsterå, L. Gunneriusson and A. Holmgren, Surface complexation modeling of
560   Fe_3O_4-H^+ and Mg(II) sorption onto maghemite and magnetite, *J. Colloid Interface*
561   *Sci.*, 2012, **386**, 260-267.

562   26.   W. Cheng, R. Marsac and K. Hanna, Influence of Magnetite Stoichiometry on the
563   Binding of Emerging Organic Contaminants, *Environ. Sci. Technol.*, 2018, **52**,
564   467-473.

565   27.   S. Bae and K. Hanna, Reactivity of Nanoscale Zero-Valent Iron in Unbuffered
566   Systems: Effect of pH and Fe(II) Dissolution, *Environ. Sci. Technol.*, 2015, **49**,
567   10536-10543.

568   28.   Y.-H. Bai, Y. Du, J.-J. Xu and H.-Y. Chen, Choline biosensors based on a bi-
569   electrocatalytic property of MnO_2 nanoparticles modified electrodes to H_2O_2,
570   Electrochem. Commun., 2007, **9**, 2611-2616.

571   29.   T. A. Kurniawan and W.-h. Lo, Removal of refractory compounds from stabilized
572   landfill leachate using an integrated H_2O_2 oxidation and granular activated carbon
573   (GAC) adsorption treatment, *Water Res.*, 2009, **43**, 4079-4091.

574   30.   N. V. Klassen, D. Marchington and H. C. E. McGowan, H_2O_2 Determination by
575   the I3- Method and by $KMnO_4$ Titration, *Anal. Chem.*, 1994, **66**, 2921-2925.

576   31.   Y. Segura, F. Martínez, J. A. Melero and J. L. G. Fierro, Zero valent iron (ZVI)
577   mediated Fenton degradation of industrial wastewater: Treatment performance and
578   characterization of final composites, Chem. Eng. J., 2015, **269**, 298-305.

579   32.   W. Zhang, H. Gao, J. He, Y. Peng and X. Xu, Removal of norfloxacin using
580   coupled synthesized nanoscale zero-valent iron (nZVI) with H_2O_2 system:
581   Optimization of operating conditions and degradation pathway, *Sep. Purif.*
582   *Technol.*, 2016, **172**, 158-167.

583   33.   W. Cheng, E. L. Kalahroodi, R. Marsac and K. Hanna, Adsorption of Quinolone
584   Antibiotics to Goethite under Seawater Conditions: Application of a Surface
585   Complexation Model, *Environ. Sci. Technol.*, 2019, **53**, 1130-1138.

586   34.   Q. Du, G. Li, S. Zhang, J. Song, Y. zhao and F. Yang, High-dispersion zero-valent
587   iron particles stabilized by artificial humic acid for lead ion removal, *J. Hazard.*
588   *Mater.*, 2020, **383**, 121170.

589   35.   H. M. Ibrahim, M. Awad, A. S. Al-Farraj and A. M. Al-Turki, Stability and
590   Dynamic Aggregation of Bare and Stabilized Zero-Valent Iron Nanoparticles
591   under Variable Solution Chemistry, *Nanomaterials*, 2020, **10**, 192.

592   36.   H. Dong and I. M. C. Lo, Influence of humic acid on the colloidal stability of
593   surface-modified nano zero-valent iron, *Water Res.*, 2013, **47**, 419-427.

594   37.   E. S. Krystofiak, E. C. Mattson, P. M. Voyles, C. J. Hirschmugl, R. M. Albrecht,
595   M. Gajdardziska-Josifovska and J. A. Oliver, Multiple Morphologies of Gold–
596   Magnetite Heterostructure Nanoparticles are Effectively Functionalized with
597   Protein for Cell Targeting, *Microsc. Microanal.*, 2013, **19**, 821-834.

598   38.   A. Liu, J. Liu, B. Pan and W.-x. Zhang, Formation of lepidocrocite (γ-FeOOH)
599   from oxidation of nanoscale zero-valent iron (nZVI) in oxygenated water, *RSC*

600   *Adv.*, 2014, **4**, 57377-57382.

601   39.   R. P. Araújo-Neto, E. L. Silva-Freitas, J. F. Carvalho, T. R. F. Pontes, K. L. Silva,
602   I. H. M. Damasceno, E. S. T. Egito, A. L. Dantas, M. A. Morales and A. S. Carriço,
603   Monodisperse sodium oleate coated magnetite high susceptibility nanoparticles
604   for hyperthermia applications, *J. Magn. Magn. Mater.*, 2014, **364**, 72-79.

605   40.   Y. Lalatonne, J. Richardi and M. P. Pileni, Van der Waals versus dipolar forces
606   controlling mesoscopic organizations of magnetic nanocrystals, *Nat. Mater.*, 2004,
607   **3**, 121-125.

608   41.   M. I. Dar and S. A. Shivashankar, Single crystalline magnetite, maghemite, and
609   hematite nanoparticles with rich coercivity, *RSC Adv.*, 2013, **4**, 4105-4113.

610   42.   S. Bae, R. N. Collins, T. D. Waite and K. Hanna, Advances in Surface Passivation
611   of Nanoscale Zerovalent Iron: A Critical Review, *Environ. Sci. Technol.*, 2018, **52**,
612   12010-12025.

613   43.   Y. Liu and G. V. Lowry, Effect of particle age (Fe^0 content) and solution pH on
614   NZVI reactivity: H2 evolution and TCE dechlorination, *Environ. Sci. Technol.*,
615   2006, **40**, 6085-6090.

616   44.   M. A. Kumar, S. Bae, S. Han, Y. Chang and W. Lee, Reductive dechlorination of
617   trichloroethylene by polyvinylpyrrolidone stabilized nanoscale zerovalent iron
618   particles with Ni, *J. Hazard. Mater.*, 2017, **340**, 399-406.

619   45.   S. Luo, T. Lu, L. Peng, J. Shao, Q. Zeng and J.-D. Gu, Synthesis of nanoscale
620   zero-valent iron immobilized in alginate microcapsules for removal of Pb(II) from
621   aqueous solution, *J. Mater. Chem. A,* 2014, **2**, 15463-15472.

622   46.   T. Yamashita and P. Hayes, Analysis of XPS spectra of Fe^{2+} and Fe^{3+} ions in oxide
623   materials, *Appl. Surf. Sci.*, 2008, **254**, 2441-2449.

624   47.   T. Radu, C. Iacovita, D. Benea and R. Turcu, X-Ray Photoelectron Spectroscopic
625   Characterization of Iron Oxide Nanoparticles, *A Appl. Surf. Sci.,* 2017, **405**, 337-
626   343.

627   48.   F. Kraushofer, Z. Jakub, M. Bichler, J. Hulva, P. Drmota, M. Weinold, M. Schmid,
628   M. Setvin, U. Diebold, P. Blaha and G. S. Parkinson, Atomic-Scale Structure of
629   the Hematite α-Fe2O3(1$\bar{1}$02) "R-Cut" Surface, *J. Phys. Chem. C*, 2018, **122**, 1657-
630   1669.

631   49.   M. Usman, M. Abdelmoula, K. Hanna, B. Grégoire, P. Faure and C. Ruby, Fe^{II}
632   induced mineralogical transformations of ferric oxyhydroxides into magnetite of
633   variable stoichiometry and morphology, *J. Solid State Chem.*, 2012, **194**, 328-335.

634   50.   J. P. Jolivet and E. Tronc, Interfacial electron transfer in colloidal spinel iron oxide.
635   Conversion of Fe_3O_4-γFe_2O_3 in aqueous medium, *J. Colloid Interface Sci.*, 1988,
636   **125**, 688-701.

637   51.   C. He, D. He, R. N. Collins, S. Garg, Y. Mu and T. D. Waite, Effects of Good's
638   Buffers and pH on the Structural Transformation of Zero Valent Iron and the
639   Oxidative Degradation of Contaminants, *Environ. Sci. Technol.*, 2018, **52**, 1393-
640   1403.

641   52. R. Marsac, S. Martin, J.-F. Boily and K. Hanna, Oxolinic Acid Binding at Goethite
642   and Akaganéite Surfaces: Experimental Study and Modeling, *Environ. Sci.*
643   *Technol.*, 2016, **50**, 660-668.
644